Journal of Petroleum
Science and Technology

Determination of Principal Permeability Directions in Reservoir Rocks from Micro-CT Data

Ahmed Zoeir[1*], Mohammad Simjoo[1], and Jafar Qajar[2]

[1] Faculty of Petroleum and Natural Gas Engineering, Sahand University of Technology, Tabriz, Iran

[2] School of Chemical and Petroleum Engineering, Shiraz University, Shiraz, Iran

ABSTRACT

The routine measurement of direction-dependent reservoir rock properties like permeability often takes place along the axial direction of core samples. As permeability is a tensor property of porous materials, it should be fully described by a tensor matrix or by three main permeabilities in principal directions. Due to compaction, cementation, and other lithification processes, which take place after sedimentation, or later distortion and fractionation of the regional earth's crust, the axial direction of core samples, may not be always one of the main permeability directions. In this paper, a computational technique to find principal permeability directions from micro-CT images of core samples was developed by us. Moreover, an assumed cube inside the core sample data with dimensions small enough to be able to imaginarily rotate inside the core limits has been chosen by us. Also, connected pore network was extracted from micro-CT data, and permeability was calculated in all space directions. In addition, stepwise rotation process continued until all possible space directions were covered. Then calculated permeabilities from all directions have been compared with each other by us. Afterwards, maximum and minimum values have been found by us. In this paper, two micro-CT datasets, which were taken from the Imperial College website, are used. Finally, the obtained results showed that the direction of maximum permeability within the carbonate core sample is about 30° deviation from the axial core direction. In addition to the main direction, the proposed computational technique can be effectively used to describe the permeability tensor of the reservoir rocks.

Keywords: Principal Permeability Directions, MATLAB, Image Analyzer App, Micro-CT Image, Rotational Cube Technique.

***Corresponding author**
Ahmed Zoeir
Email: ah_zoeir@sut.ac.ir
Tel: +98 41 3344 9150
Fax: +98 41 3344 4355

Article history
Received: November 02, 2017
Received in revised form: March 07, 2018
Accepted: April 24, 2018
Available online: February 16, 2019
DOI: 10.22078/jpst.2018.2966.1482

INTRODUCTION

X-ray micro-computed tomography (micro-CT) has now been widely used in petroleum research. One of the main advantages of the micro-CT technique is that it is non-destructive, i.e. core samples do not expose to damage during CT scanning while in routine experimental methods, core samples are usually affected by fluids and test conditions, or even they may lose their original properties. CT scanning technique can provide valuable information about fluid flow through porous media, e.g. in IOR/EOR research and rock properties, in particular porosity and permeability. Permeability is inherently a function of the internal structure of the rock sample, i.e. it mainly depends on tortuosity, pore aspect ratio, and topology. In fact, no accurate relationships exist to correlate permeability of real rocks to pore-scale parameters, although several simplified correlations have been proposed. The capability of the micro-CT method has motivated investigators to predict permeability through the application of numerical techniques to describe fluid flow through porous media. To perform such a precise numerical modeling, the internal structure of the porous medium needs to be determined either by reconstruction of the porous medium via thin section data or CT data of the porous media to obtain a 3D image of the pore space [1]. Most of the available methods to predict permeability from micro-CT data of core samples are nodal, treating the micro-CT images voxel by voxel. Mo-st image-based permeability calculations have been based on the Lattice-Boltzmann method which applied different finite element (or finite difference) algorithms to solve the governing equations within porous media [2]. The Lattice-Boltzmann method to obtain absolute permeability of unconsolidated and consolidated rocks was used by Jin et al [3]. Lattice-Boltzmann method to model reactive flow through porous media was applied by Kang et al. The phases of minerals and fluid and activated advection and diffusion process within their model were considered by them [4].The static and also flow properties of sandstone samples with high resolution micro-CT tomography images were estimated by Knackstedt et al [5] two pore scale approaches, Lattice-Boltzmann, and Pore-Network modeling to simulate single phase flow and its properties in made sphere packing in different realizations were used by Pan et al [6]. Also, two fluid phase porous media systems comprised of a synthetic packing with a relatively uniform distribution of spheres have been simulated by Pan et al, and they tried to estimate permeability for that system [7]. Lattice-Boltzmann method to obtain rock permeability in different directions using high resolution X–ray tomography images has been used by Piller et al [8]. Although Lattice-Boltzmann is a powerful, widely used approach, it needs huge computational resources (high CPU/Memory/RAM) to perform numerical calculations, thus requires the use of massively parallel computational resources. Moreover, applying no-slip or constant pressure boundary conditions is not straightforward [9,10]. The finite-difference and Lattice-Boltzmann methods to calculate the permeability of three dimensional porous media were compared by Manwart et al. It was shown by them that in terms of memory, the Lattice-Boltzmann method requires 2.5 times more memory than what was required by finite-difference method, while the computation time, and numerical results of the two methods were similar [11]. The finite-difference method has been

applied several times to predict permeability. Also, a finite-difference method to solve for flow using a parabolized Stokes formulation where the pressure is assumed to vary only in the main direction of flow was applied by Oren and Bakke [12]. Moreover, the same method for predicting the permeability of North Sea chalk was applied by Kainourgiakis et al, and a good agreement with experimental measurements was shown by Kainourgiakis et al [13]. The permeability of slices which was taken through micro-CT (computed tomography) images of a sandstone was estimated by Silin and Patzek estimated by Silin and Patzek. Afterwards, the image permeability by taking the harmonic mean of the slices was estimated by Silin and Patzek [14]. Moreover, in anisotropic porous media with unknown principal directions, horizontal and vertical permeabilities often give an incomplete description of porous media transmissibilities. In addition to that, laboratory experiments are often capable to determine permeability only along core axes or transverse direction. In this paper, a processing method for obtaining the directional permeability of the reservoir rock samples using two micro-CT images which were downloaded from the Imperial College website was provided by us [15]. For doing this, an in-house program using MATLAB software (R2015a) was developed by us, and the permeability results for two sets of micro-CT image of sandstone and carbonate samples were developed by us. The novelty of this study is that the permeability in all possible space directions was calculated by us, and the main directions to fully describe the permeability tensor was specified by us. In addition, section-wise point of view enables us to perform calculations using less computational resources. Then the results must be processed to upscale for real reservoir extents using some statistical methods. One must notice that in situations in which core plugs are limited or reservoirs with major log records, a core digital analysis gives limited information and it cannot be used for reservoir rock property predictions.

EXPERIMENTAL PROCEDURES COMPUTATIONAL METHODS

In this paper, a rapid and easy-to-use (or user-friendly) method to obtain directional permeability using digital micro-CT image data of the core samples were introduced by us. In order to minimize the processing runtime, one major factor is to segment the micro-CT images in order to reduce the size of micro-CT (computed tomography) image data to REV (representative elementary volume) of each special target property. Each porous media property such as porosity and permeability could have its own REV. For obtaining REV from the micro-CT (computed tomography) image data, a growing cubic control volume within the porous media was assumed by us. The cubic volume started expanding from one fixed voxel in the 3D digital image, and its dimensions increased continuously while its porosity and permeability were determined at the same time. When the calculated value of each property (porosity and permeability) converged to a fixed value with a certain tolerance, the volume expansion terminated, and then the resulting volume is reported as the REV of that property. Also, in this paper, all the directional permeability calculations are performed on REV volumes to significantly reduce the process runtimes. In Figure 1, MATLAB's three dimensional representation of the permeability REV within two case studies, namely sandstone and carbonate micro CT files which have been extracted from full CT images is shown.

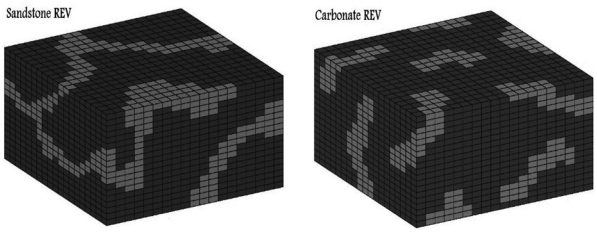

Figure 1: MATLAB presentations of sandstone and carbonate REV which shows pore and grain voxels.

Another factor which can enormously influence the computational runtime is applying neighborhood operation on the calculation procedure. This means that the images are divided into a number of neighboring segments, and calculations are performed on each segment, rather than processing the entire segmented image at once. In this manner, a specified functions is used to process each neighbor, the extracted information of one neighbor is fed to the next one, and results from all the neighbors are reassembled to give overall results. It is important that you pay attention to the following tip that several predefined MATLAB functions use neighborhood operation as their default.

In this paper, micro-CT data in the format of Net CDF (network common data format) were used by us. In order to use the predefined functions and modules of the image processing toolbox of MATLAB for the Net CDF file, the 3D micro-CT image data to a series of 2D image data were converted by us. For the calculation of porosity, the MATLAB binary mask is applied to divide voxels into two groups of pores and solids. Function's threshold with respect to RCAL experimental reported data in order to calibrate the micro-CT data was adjusted for us, and it was used for the calculation of the directional permeabilities.

Moreover, properties like average throat size, surface area, and porosity can be calculated from separated 2D images, while flow properties like permeability cannot, because the pore connected network cannot be extended from 2D to a 3D domain. Instead, the morphological reconstruction part of the image processing toolbox of MATLAB to obtain connected pore network over 3D CT images has been used by us. In this software, it is also possible to choose the connectivity method of the voxels. Also, the six-connected option for the voxels which is widely applied to obtain pore connectivity within the reservoir rock micro-CT data process is used by us. In this manner, each voxel can be connected to neighborhood voxels only on each of cube faces, not edges or corners. After the elimination of the isolated pores, the remaining voxels construct the connected pore network. Then, the Stokes equation is solved through the network to obtain fluid linear velocity within each pore. To aim this, pore voxels as close ducts have been treated by us, and their average hydraulic diameters have been found by us. Then, to accurately calculate permeability in X, Y, and Z directions, a distinction (or differentiation) between flow in individual pores and in groups of pores has been made by us. When connected groups of pores are exposed to a pressure difference, pores which are in contact with solid phase obey the no-slip condition rule and have the smallest flow velocities, while those located in the center of the group have the largest linear velocities. The Euclidean distance transform mapping is a solution to treat this conflict. It assigns zero number to pore voxels which are in contact with a solid phase, and larger numbers to pore voxels which are farther from the solid phase. This number grows as voxel distance from solid phase increases. Finally, the velocity distribution in all points of porous media can be obtained by multiplying distance transform numbers with linear velocities calculated from the

Stokes equation. To obtain permeabilities, hypothetical sections perpendicular to the flow direction have been assumed by us, as is shown in Figure 2.

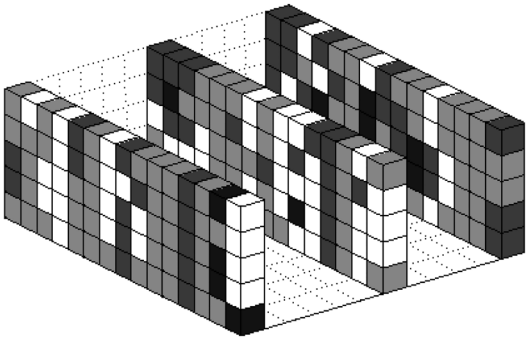

Figure 2: A schematic of perpendicular resistance sections in the assumed flow direction.

Each section applies its own resistance to flow, which is proportional to its pore voxel allotment within the whole segmented image. Actually, it is supposed by us that no pressure difference exists in sections perpendicular to flow direction. This section-wise point of view helps reducing computational resource requirements, and hence the runtime of calculations. Each section has a different pressure drop around itself, while a fixed volumetric flow rate passes through all sections. The volumetric flow rate is evaluated with Darcy's law for each section. Then Darcy's law is written for the full-segmented image, and permeability is calculated in the desired direction from the equation. In order to cover all the possible space directions, the cube was rotated stepwise in x-direction while also turned around the x-coordinate to cover all possible z and y directions. One cubic control volume with the size of permeability REV is considered within the center of the micro-CT data. Then all its eight corners were transported to new positions via desired degree rotational process. Moreover, their resultant locuses were calculated using Spherical coordinates. These new eight corners formed the newly superimposed volume now contains fresh micro-CT voxels. Here, flow direction from one face of the newly appeared cubic control volume to the opposite face was supposed by us, and the connected pore network along this direction was extracted by us. After each calculation, the superimposed control volume was rotated stepwise, and the connected pore network was extracted from micro-CT data. Moreover, permeability was calculated in each of these space directions. Stepwise rotation process continues until all possible space directions are covered. The number of steps depends on the desired precision and allowable time of calculations that in turn depends on the available computational hardware. Then calculated permeabilities from all directions were compared with each other by us. Afterwards, maximum and minimum values were found by us. These direction-dependent permeabilities can be used as the principal directions to present the permeability tensor. An In-house code was written with MATLAB GUI using its toolboxes to calculate core properties from micro-CT data, as shown in Figure 3. Written MATLAB code was capable to determine absolute and connected porosities, pore and throat size distributions, REVs of porosity, and permeability in sandstone and carbonate case studies, pressure distribution around assumed cross sections along the flow direction, and direction of maximum and minimum absolute permeabilities within micro-CT data.

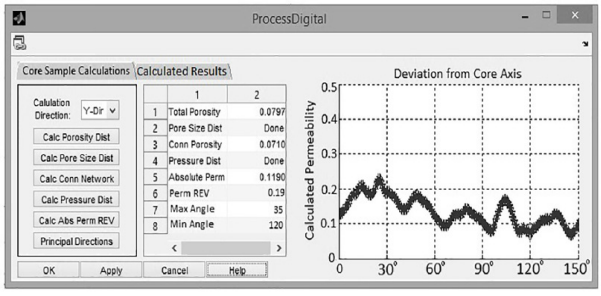

Figure 3: An image of the GUI of the developed MATLAB code to calculate core properties from image data.

RESULTS AND DISCUSSIONS

At first stage of the computational procedure, the representative elementary volumes of porosity and permeability were needed to be determined. In this regard, three random voxels were selected in the micro-CT image of the rock sample, namely segmented parts 1, 2, and 3. Then the volume of each segmented part was expanded, and the corresponding porosity and permeability values were obtained. Also, an increase in volume size continues until finally, the calculated porosity and permeability reach relatively constant values. The volume which corresponds to such constant values of porosity, and permeability has been considered as the REVs. In addition, the results summary of the computations performed to obtain the REVs of porosity and permeability in the sandstone core sample, are shown in Table 1.

Table 1: Computational procedure to obtain REV in the sandstone core sample.

	Voxel volume (in^3)	0.05^3	0.2^3	0.5^3	0.8^3		Voxel volume (in^3)	0.2^3	0.5^3	1^3	2^3
Calculated porosity (%)	Segmented part 1	13.6	12.2	11.0	11.1	Calculated permeability (Darcy)	Segmented part 1	0.45	0.40	0.35	0.36
	Segmented part 2	9.5	10.5	11.1	11.2		Segmented part 2	0.20	0.29	0.37	0.38
	Segmented part 3	14.1	12.4	10.9	11.0		Segmented part 3	0.49	0.42	0.33	0.34
	Average value	12.4	11.7	11.0	11.1		Average value	0.38	0.37	0.35	0.36

For all the three randomly selected voxels, as the volume expands from 0.053 in^3 to 0.53 in^3, the calculated porosity tends to reach a constant value of 11±0.1%. When the volume increases further to 0.83 in^3, no significant change is visible in the calculated porosities. Thus 0.53 in^3 is determined as REV of porosity in the sandstone core sample. The main reason that the calculated porosity of segmented part 2 is always smaller than the average value is that the segmented parts 1 and 3 started expanding from the pore cumulated area while the segmented part 2 started to expand from an area mostly consists of grains. The same procedure was applied to calculate the permeability REV using expanding volumes from randomly selected voxels. The results showed that the segmented parts' permeabilities converged to a constant value of 0.35±0.02% Darcy as the volume increased from 0.23 to 13 in^3. As the voxel volume increased further to 23 in^3, no significant changes appear in the calculated permeabilities. Thus 13 in^3 is determined as REV corresponding to the permeability of the sandstone core sample. It is noticeable that the REV values of porosity and permeability for the sandstone case study were different. In addition, permeability of REV which is calculated to some amounts is larger than porosity of REV.

By knowing REV, three parts within full sandstone image, which are slightly larger than REV volumes, have been segmented by us for two reasons: first, (1) to ensure representativeness of the calculated properties, and second, (2) to reduce runtime and RAM requirements. In order to calculate the properties of the sandstone sample, three new segmented parts within the sandstone micro-CT image were selected by us. The volume of segmented parts was selected slightly larger than REV to avoid long runtime problems and also to reduce high RAM requirement. In Table 2, the calculated properties from micro-CT data processing in sandstone case study are shown.

Table 2: Calculated characteristics of sandstone rock sample with the digital image processing method.

Porous media characteristic		Porosity	Pore size	Throat size	X-Dir Perm	Y-Dir Perm	Z-Dir Perm
Calculated values	Segmented part 1	11.3	75 µm	35 µm	0.35	0.37	0.08
	Segmented part 2	11.1	70 µm	30 µm	0.33	0.35	0.10
	Segmented part 3	11.5	75 µm	35 µm	0.36	0.34	0.06
	Average value	11.3	73 µm	33 µm	0.35	0.35	0.08
Reported value from experiment		10.5	-----	-----	0.30	0.30	0.10

As shown in Table 2, comparisons of the average calculated porosity with a value of 11.3±0.2%, from the micro-CT data processing and the experimental reported value of 10.5%, showed a good agreement. Similarly, the permeability values obtained from micro-CT data process, 0.35 (X,Y-direction), and 0.08 (Z-direction) were also close to reported values of 0.3 (X,Y-direction) and 0.1 (Z-direction). The difference between calculated permeabilities with experimentally reported permeabilities, is due to the fact that individual pores show high capillary pressures, and do not respond to the pressure gradient along the flow direction, but high capillary forces in individual pores are not considered by us. To find out the REV volumes of porosity and permeability for carbonate sandstone, this time within carbonate micro-CT data, three random voxels are again chosen. Also, control volumes to find out REVs have been expanded by us. Results are shown in Table 3.

Table 3: Calculated characteristics of carbonate rock sample versus porous media volume size.

Porous Media Volume Size (cubic inches)		0.01^3	0.02^3	0.05^3	0.2^3	Porous Media Volume Size (cubic inches)		0.02^3	0.05^3	0.2^3	0.5^3
Calculated Porosity (%)	Segmented Part 1	13.6	12.2	8.2	8.1	Calculated Permeability (Darcy)	Segmented Part 1	0.35	0.25	0.19	0.14
	Segmented Part 2	13.1	10.4	8.1	8.0		Segmented Part 2	0.33	0.19	0.15	0.13
	Segmented Part 3	4.8	6.5	8.0	7.9		Segmented Part 3	0.07	0.10	0.14	0.12
	Average	10.5	9.7	8.1	8.0		Average	0.25	0.18	0.16	0.13

As is shown in Table 3, in all three randomly chosen expanding parts, the calculated porosities tend to a constant value of 8%. Moreover, calculated porosities converge to constant values at volumes about 0.05^3 cubic inches (Porosity REV). The reason that the tabulated results of chosen parts number 3 is always smaller than final value is that this part starts expanding from a grains cumulated area while conversely parts 1 and 2 do not. Same converging procedure happens when expanding control volume to calculated permeability of all chosen parts is considered. This time permeability values converge to constant amount of 0.13 Darcy after volumes grow to 0.2^3 cubic inches. The REV of permeability in carbonate case study again differs from REV of porosity and has the value of 0.2^3 cubic inches.

By knowing REV, three parts within full carbonate core image, which are slightly larger than REV volumes, were again segmented for two reasons (by us): first, (1) to ensure representativeness of the calculated properties, and second, (2) to reduce the runtime and RAM requirements. Calculated parameters for carbonate case study are shown in Table.4.

Table 4: Calculated characteristics of carbonate rock sample with the digital image processing method.

Porous Media Characteristic		Porosity	Pore Size	Throat Size	X-Dir Perm	Y-Dir Perm	Z-Dir Perm
Calculated Values	Segmented Part 1	8.1	35 µm	15 µm	0.13	0.14	0.08
	Segmented Part 2	8.0	32 µm	19 µm	0.11	0.10	0.03
	Segmented Part 3	8.2	31 µm	17 µm	0.15	0.15	0.05
	Average	8.1	33 µm	17 µm	0.13	0.13	0.05
Experimental Values		7.5	-----	-----	0.1	0.1	0.05

The average values of the pore and also throat sizes are determined from micro-CT images of the carbonate sample, similar to sandstone case study. By making a comparison between the results of Table 4 and

Table 2 showed that the average pore sizes and also throat sizes are smaller in the carbonate sample in comparison to sandstone sample. Pore and throat size results are satisfied with sandstone and carbonate permeabilities. As carbonate sample with smaller throats has the smaller permeability in comparison to sandstone sample.

After that, our imaginary cube of size REV was rotated (by us) inside three-dimensional micro-CT data stepwise around X-axis. Also, for each step, Y and Z-axes in a plane perpendicular to X-axis was rotated by us. Moreover, this procedure covers all possible directions in space with a step of 30° in all three Cartesian directions.

The results showed that the main direction of minimum permeability is the same as the original Z-direction which is taken vertical downward. Permeabilities in horizontal plane is maximum although East-West direction is chosen by you. In other words, results for this case study showed that the core is taken in the direction of sedimentation and compaction. Of course, more detailed calculations, (i. e. smaller step sizes) may lead to more precise determination of the directions of maximum and minimum permeabilities. Results are presented in Table 5.

Table 5: Calculated permeabilities of sandstone rock sample after rotation of imaginary cube in space.

YZ Plane Rotation Angle		0°	30°	60°	90°	210°	240°	270°
X Axis Rotation Angle = 0°	Y-Dir Perm	0.35	0.24	0.15	0.08	0.16	0.25	0.35
	Z-Dir Perm	0.08	0.19	0.28	0.35	0.27	0.18	0.08
X Axis Rotation Angle = 30°	Y-Dir Perm	0.33	0.29	0.25	0.18	0.26	0.31	0.35
	Z-Dir Perm	0.17	0.21	0.29	0.35	0.30	0.23	0.16
X Axis Rotation Angle = 60°	Y-Dir Perm	0.34	0.31	0.29	0.26	0.28	0.30	0.33
	Z-Dir Perm	0.27	0.30	0.32	0.35	0.33	0.30	0.28
X Axis Rotation Angle = 90°	Y-Dir Perm	0.35	0.34	0.35	0.35	0.34	0.35	0.35
	Z-Dir Perm	0.35	0.35	0.33	0.35	0.35	0.33	0.34

Such calculations are also performed on micro-CT data of carbonate case study which shows a little difference in results. The results showed that the principal directions of maximum and minimum permeabilities differ from original directions for about 30°. As indicated in Table 6, when the X-axis rotates from 0° to 30°, calculated permeability in Z direction decreases while permeability in X and Y directions increase. The additional rotation will tend to change in opposite direction. Results showed that the direction of the minimum permeability has deviated from the original direction 30° with respect to X-axis and 30° with respect to Z-axis. Conversely, maximum permeability perpendicular to the minimum permeability direction in all three coordinates.

Calculated results can be evaluated with the measurement of transverse permeability in a direction perpendicular to core axis. Unfortunately, case studies' data do not cover this values but the permeability in core axis direction is satisfied with experimental values, and exactly the same procedure of estimation is applied for all several directions, so the authors believe that the calculated permeabilities in all directions are in agreement with the experimental results.

This difference between principal directions and main directions in which core sample which is taken shows geological activities after sedimentation processes, thus the related formation layer is no more horizontal, and its direction is changed with some significant angles.

Table 6: Calculated permeabilities of carbonate rock sample after rotation of imaginary cube in space.

YZ Plane Rotation Angle		0°	30°	60°	90°	210°	240°	270°
X Axis Rotation Angle = 0°	Y-Dir Perm	0.13	0.10	0.07	0.05	0.03	0.09	0.13
	Z-Dir Perm	0.05	0.08	0.11	0.13	0.15	0.10	0.05
X Axis Rotation Angle = 30°	Y-Dir Perm	0.13	0.15	0.10	0.07	0.02	0.08	0.13
	Z-Dir Perm	0.03	0.02	0.08	0.12	0.15	0.09	0.03
X Axis Rotation Angle = 60°	Y-Dir Perm	0.13	0.09	0.06	0.05	0.03	0.10	0.13
	Z-Dir Perm	0.06	0.07	0.10	0.12	0.14	0.09	0.05
X Axis Rotation Angle = 90°	Y-Dir Perm	0.13	0.15	0.12	0.10	0.11	0.12	0.13
	Z-Dir Perm	0.13	0.11	0.12	0.13	0.12	0.11	0.13

CONCLUSIONS

Several key finding of the present paper can be summarized as follows:

(1) Due to volume reduction of micro CT data to REV and also neglecting changes in planes perpendicular to the supposed flow direction, the proposed method was capable to calculate permeability within several space directions via available RAM and CPU of personal computers. Since these simplification assumptions were considered by us, the calculations give reasonable results in comparison with experimentally reported permeability values.

(2) To determine permeability from grayscale images, one must first perform a check over critical intensity that fits porosity of the rock, and then apply this critical intensity for permeability calculations. In our case studies, pixels with 90 or smaller intensities as pore to cover saturated phase pixels into the pore phase were assumed by us.

(3) Exact estimations of rock permeability may be achieved when EDT mapping is used in the image data. Euclidean distance transform can be applied for various velocities for different pore pixels; pixels which are in contact with solid phase have small velocities while those in the center of pore have biggest values.

(4) In processing 3D digital images with MATLAB, if possible, we advise reducing input data amount to representative elementary volume (REV) of permeability to avoid additional unnecessary RAM usage. Also, in coding procedures, if needed, it is recommended not to define multidimensional matrixes which are larger than the original image size. Moreover, it is recommended to use unavoidable input data as the largest matrix in the program.

(5) Quick property calculations on image data using MATLAB can be reached when working with its image processing toolbox predefined functions. In addition, determining the contact area, providing a connected pore network, Euclidean distance transform mapping, and calculation of representative volumes, all have predefined functions in image processing toolbox of MATLAB. Finally, make sure your desired function is not available by default before trying to write your own program.

ACKNOWLEDGEMENTS

Authors acknowledge the free support of micro CT image files by the Imperial College website, www.imperial.ac.uk, World Wide Web.

NOMENCLATURES

CT	: Computed Tomography
REV	: Representative Element Volume

REFERENCES

1. Dong H. and Blunt M. J., "Pore Network Extraction from Micro Computerized Tomography Images," *Journal of Physical Review E*, **2009**, *80*, 36307-36318 .
2. Blunt M. J., "Flow in Porous Media: Pore Network Models Multiphase Flow," *Curr Opin Colloid Interface Science*, **2001**, *6*, 197-207.
3. Jin G., Patzek T. W., and Silin D. B., "Direct Prediction of Absolute Permeability of Unconsolidated and Consolidated Reservoir Rocks," *Proceedings of the SPE Annual Technical Conference Exhibition*, Heuston, Texas, SPE 90084, **2004**, 1-15.
4. Kang Q., Lichtner P. C., and Zhang D., "Lattice Boltzmann Pore Scale Model for Multicomponent Reactive Transport in Porous Media," *Journal of Geophysics Research 111*, B05203, **2006**, *2*(5), 545-563.
5. Knackstedt M. A., Arns C. H., Limaye A., Sakellariou A., and et al., "Digital Core Laboratory: Properties of Reservoir Core Derived from 3D Images," Proceedings of *the SPE Asia Pacific conference on integrated modelling or asset management*, KualaLumpur, Malaysia, SPE 87009, **2004**.
6. Pan C., Hilpert M., and Miller C. T., "Pore Scale Modeling of Saturated Permeabilities in Random Sphere Packings," *Physical Review E*., **2001**, *64* (6).
7. Pan C., Hilpert M., and Miller C. T., "Lattice Boltzmann Simulation of Two-phase Flow in Porous Media," *Journal of Water Resources Research*, **2004**, *40*(1), 1-14.
8. Piller M., Schena M., Nolich S., Favretto F. and et al., "Analysis of Hydraulic Permeability in Porous Media: from High Resolution X-ray Tomography to Direct Numerical Simulation," *Transp. Porous Media*., **2009**, *80*, 57-78.
9. D'Humieres D. and Ginzburg I., "Viscosity Independent Numerical Errors or Lattice-Boltzmann Models: from Recurrence Equations to Magic Collision Numbers, *Comput. Math. Appl*., **2009**, *58*, 823-840.
10. Noble D. R., Chen S., Georgiadis J. G., and Buckius R. O., "A Consistent Hydrodynamic Boundary Condition for the Lattice-Boltzmann Method," *Physics of Fluids, AIP Publishing*, **1995**, *7*, 203-210.
11. Manwart C., Aaltosalmi U., Koponen A., Hilfer R., and et al., "Lattice Boltzmann Finite-difference Simulations for the Permeability for Three-dimentional Porous Media," *Physical Review E.*, **2002**, *66*, 16702-16713.
12. Oren P. E. and Bakke S., "Process Based Reconstruction of Sandstones Prediction of Transport Properties," *Transp. Porous Media*, **2002**, *46*, 311-343.
13. Kainourgiakis M. E., Kikkinides E. S., Galani A., Charalambopoulou G. C., and et al., "Digitally Reconstructed Porous Media: Transport Sorption Properties," *Transp. Porous Media*, **2005**, *58*, 43-62.
14. Silin D. B. and Patzek T. W., "Predicting Relative-permeability Curves Directly from Rock Images," *Proceedings of SPE Annual Technical Conference Exhibition*, New Orlean, LA, SPE 124974, **2009**.
15. Imperial College, London, UK: PERM, Petroleum and Rock Mechanics Group. Available from: www.imperial.ac.uk/. Accessed **2017**.